



Article

The Rapid Boiling of Thin Liquid Films with Different Thicknesses on Nanochannel Copper Plates: A Molecular Dynamics Study

Nini Wu ^{1,2} , Liangcai Zeng ^{2,3}, Ting Fu ^{2,3,*}, Juan Chen ^{1,2}, Feng Zhang ^{2,3} , Yun Zeng ^{1,4} and Shuai Peng ⁵

¹ Key Laboratory of Metallurgical Equipment and Control Technology, Ministry of Education, Wuhan University of Science and Technology, Wuhan 430081, China; niniwu@wust.edu.cn (N.W.)

² Precision Manufacturing Institute, Wuhan University of Science and Technology, Wuhan 430081, China

³ Hubei Key Laboratory of Mechanical Transmission and Manufacturing Engineering, Wuhan University of Science and Technology, Wuhan 430081, China

⁴ School of Mechanical Engineering, Yangtze University, Jingzhou 434000, China

⁵ College of Technology, Hubei Engineering University, Xiaogan 432000, China

* Correspondence: futing1234gh@wust.edu.cn

Abstract: Boiling heat transfer on nanostructured surfaces presents great potential in cooling highly integrated microelectronic devices. Analysis of the factors affecting boiling heat transfer included the analysis of nanostructure and wettability, indicating that consideration of the influence of working liquid quantity is essential in finite spaces. Rapid boiling water films with various thicknesses placed on the same nanochannel copper plate were studied via molecular dynamics (MD) simulations. The simulation results reveal that the potential energy difference in the vapor–liquid coexisting region on the nanochannels was lower for thicker films, and the evaporation rate was lower. The effect of water film thickness on boiling heat transfer is closely related to the potential energy difference in the vapor–liquid coexisting region on the nanochannels. The heat transfer effect was the worst in case 1, where the water thickness was lower than the height of the nanochannels. This is because there is no guaranteed liquid replenishment at the nucleation points, although the potential energy difference was greatest in the vapor–liquid coexistence zone of case 1. Evaporation was the greatest in case 2, where the water film just covered the nanochannels because of the larger potential energy difference and sufficient liquid water replenishment. This study is of great significance for the analysis of the vapor–liquid flow mechanisms of micro/nanostructured surfaces and the improved design of thermal management equipment of micro/nano devices.

Keywords: heat transfer; boiling; nanochannel; different thicknesses; molecular dynamics



Citation: Wu, N.; Zeng, L.; Fu, T.; Chen, J.; Zhang, F.; Zeng, Y.; Peng, S. The Rapid Boiling of Thin Liquid Films with Different Thicknesses on Nanochannel Copper Plates: A Molecular Dynamics Study. *Coatings* **2023**, *13*, 2057. <https://doi.org/10.3390/coatings13122057>

Academic Editor: Angela De Bonis

Received: 23 October 2023

Revised: 3 December 2023

Accepted: 6 December 2023

Published: 8 December 2023



Copyright: © 2023 by the authors. Licensee MDPI, Basel, Switzerland. This article is an open access article distributed under the terms and conditions of the Creative Commons Attribution (CC BY) license (<https://creativecommons.org/licenses/by/4.0/>).

1. Introduction

Heat transfer for liquid–vapor phase transitions in thin liquid films can rapidly decrease the interface surface temperature in narrow spaces [1], with the technique being widely used in microelectronic thermal management [2]. Micro-scale boiling heat transfer faces significant challenges in light of the rapid development of microelectronic fabrication technologies because of the surge in microelectronic integration and heat flux. Meanwhile, heat-transfer-strengthening technology has attracted considerable attention in recent years [3–6].

Most current experimental and simulation research methods focus on enhancing boiling heat transfer by changing the solid surface characteristics, such as morphology and wettability, which are effective in many boiling-strengthening applications [7,8]. Cao et al. [9] showed that the heat transfer coefficient on surfaces modified with Cu–Zn nanoparticles was significantly enhanced compared with that on smooth surfaces. Liu et al. [10] found that the critical heat flux (CHF) of micro/nanostructured surfaces increased with

subcooling, which is greatly affected by the spacing of the surfaces. Shen et al. [11] found that the heat transfer coefficients of hybrid wettable surfaces were greater than those of uniform wettable surfaces. These experimental studies indicate that surface modifications play important roles in enhancing heat transfer. However, wettability and roughness always coexist and influence each other in experiments [12,13].

Wettability can also be controlled through the use of surface nanostructures [14,15]. The effective mechanism of modified surface characteristics from a microscopic heat transfer perspective is unclear, and classic heat transfer theories are no longer feasible at such small scales due to failures of the continuum assumption. As an advanced simulation method, the molecular dynamics (MD) method is widely used in microscopic heat transfer research [16–18] as it successfully captures atomic trajectories, energy transfer information, and information on heat transfer mechanisms. Wang et al. [19] used MD and found that bubbles move faster when micro/nanostructures are modified through improvements to the CHF. Increasing the solid–liquid contact area through greater nanochannel heights on copper plates significantly enhanced heat flux [20] and nucleation [21] during the explosive phase transition in MD simulations. However, the heat transfer of nanostructures with larger solid–liquid contact areas was poor as it was affected by the location of the nanostructure, especially the spacing between each surface [22]. An optimal scheme exists for the spacing of nanostructures and flat surfaces [23,24]. Chen et al. [25] used MD simulations to show that nanostructured surfaces improve the heating intensity and nucleation rate. However, the temperature heterogeneity generated on the surface was not why the micro/nanostructure was conducive to the formation of nucleation points.

Most of the above scholars focused on improving the heat dissipation surface in nanostructures with different design methods employed to strengthen the heating surface. The fundamental influencing factors of enhanced boiling heat transfer include an increased solid–liquid contact area, number of nucleation points, and liquid supply between them in all of these strengthening methods [23]. These influencing factors can be varied through the surface characteristics and the amount of working liquid.

Shavid et al. [21] found that the temperature of working fluids increases rapidly during explosive boiling when the nanostructure height is equal to or more than the liquid layer thickness. Fan et al. [26] showed that evaporation differed significantly at the solid–liquid interface and at the channel center due to evaporation-driven liquid flow through the nanochannels. Therefore, the working liquid film thickness in the nanochannel plate surface is predicted to significantly affect the boiling heat transfer due to a changing solid–liquid contact area and solid–liquid supply. Working liquid films with different thicknesses significantly influence the heat transfer of nanostructured surfaces. However, there are few studies on the effect of changing liquid thickness on the heat transfer caused by the vapor–liquid flow on the surface of nanostructures, which is particularly important for the design of thermal management devices in micro–nano systems. In particular, Hanks et al. [27] designed a profiled structure thermal management device to deal with ultra-high heat flux by using nano-sized pores to generate large negative pressure to allow for the continuous flow of liquid into nucleation points. Recently, Li et al. [28] proposed an innovative method of regulating vapor–liquid to enhance flow boiling heat transfer.

The improvement in micro/nanostructured surface thermal management performance has been the focus of many scholars. In this paper, boiling heat transfer simulations employing four different liquid film thicknesses on the same nanochannel copper plate are studied with MD. Variations in the solid–liquid temperature and the evaporation rate of the working liquid are compared, emphasizing the density and energy distribution of water molecules in the vapor–liquid coplanar region above the nanochannels. What is more, the optimal working liquid quantity is determined, and the vapor–liquid flow mechanism is determined in the vapor–liquid coexistence region of the nanochannels. In contrast to many researchers aiming to enhance heat transfer by improving surface modification, in this study, the effects of different quantities of working liquid on the thermal management properties of micro/nanostructured surfaces were studied, and the

vapor–liquid flow mechanism in the vapor–liquid coexistence zone for enhanced boiling on the nanochannel surface was analyzed from the perspective of energy. The results of this study provide theoretical support for improving the design of micro–nano thermal management equipment.

2. Simulation Models and Methods

A simulation box ($86.64 \text{ \AA}(x) \times 86.64 \text{ \AA}(y) \times 270.75 \text{ \AA}(z)$), as shown in Figure 1, was built. Water was modeled as the working fluid using a four-site water model (TIP4P) [29,30], while a nanochannel copper plate was modeled as the heated solid with six copper layers (height = 10.83 \AA) and two rectangular channels (height = 32.49 \AA). Four different water molecule quantities, 4760 (case 1), 5916 (case 2), 7072 (case 3), and 8228 (case 4), were placed on the same nanochannel copper plate for boiling heat transfer simulations.

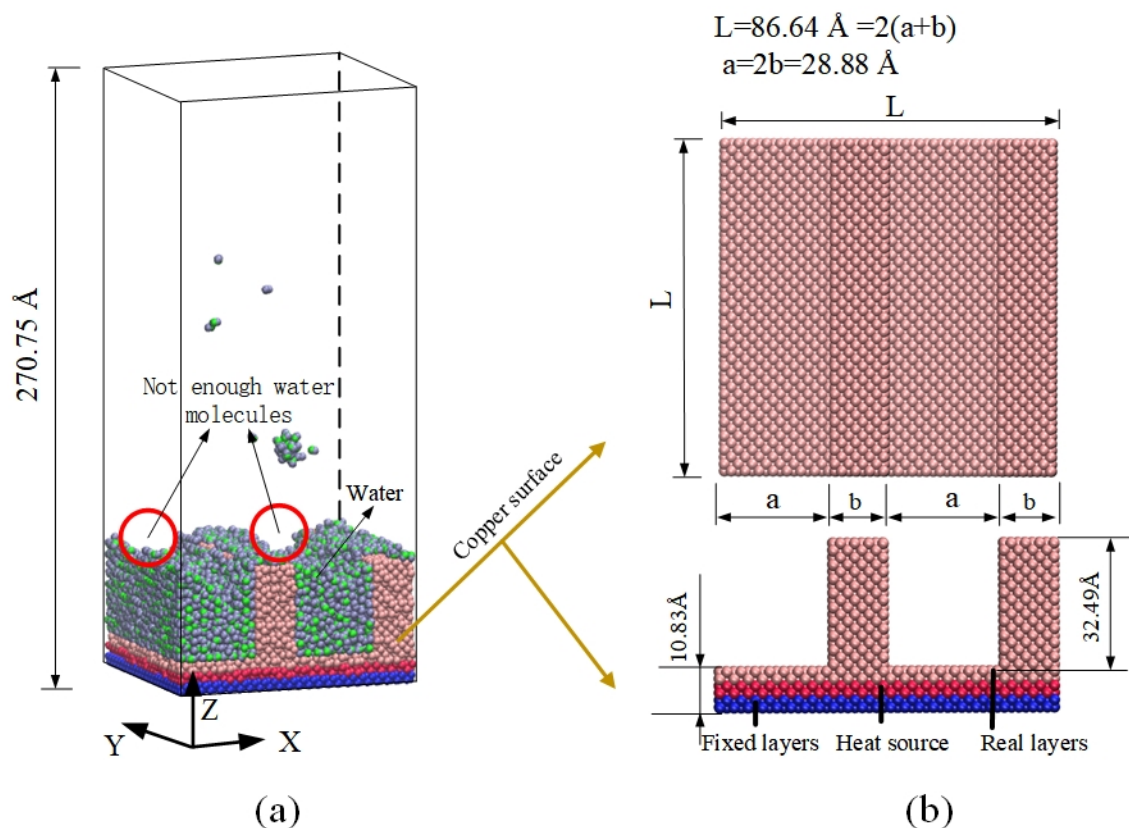


Figure 1. Schematic diagram of (a) the initial configuration of the simulation for case 1 and (b) a view of the nanochannel copper plate.

The initial simulation configuration for case 1 had 4760 water molecules placed above a nanochannel copper plate, as shown in Figure 1a. However, there were insufficient water molecules to completely cover the nanochannels, as shown by the red circles. Figure 1b illustrates the fixed layers at the bottom that prevented atomic migration for six copper layers. The simulations in this paper are divided into three steps: (1) The energy of the system is minimized and equilibrated to a stable state at a temperature of 298 K under a Langvin thermostat. (2) The two middle layers are the heat source maintained and stabilized at 1000 K via a Langevin thermostat. This temperature is high enough with respect to the critical temperature of water (373 K) to achieve rapid boiling. (3) The water molecules with the minimum energy level at 298 K are placed above the real layers with a high thermal level, including the top two layers and nanochannels through which heat is transferred to the liquid water with an initial temperature of 298 K.

Periodic boundary conditions were applied along the X- and Z-directions; meanwhile, the mirror boundary condition was used in the Z-direction. The whole system was set up in

the microcanonical ensemble (NVE). A time step of 1 fs was used for all simulations, which were performed with the open-source code LAMMPS (Large-scale Atomic/Molecular Massively Parallel Simulator), and data visualization was carried out with VMD (visual molecular dynamics) [31]. Potential functions are related to the nature of the molecular force and describe forces between atoms. In the simulations, the Lennard–Jones (L–J) 12–6 potential [32] was used in Cu–O atoms and Cu–Cu atoms and is given as

$$U = 4\epsilon \left[\left(\frac{\sigma}{r} \right)^{12} - \left(\frac{\sigma}{r} \right)^6 \right] \quad (1)$$

where ϵ denotes the distance of the potential well and σ is the finite length where the potential energy is zero. The interactions between H–Cu and H–H atoms were ignored and assumed to be zero [33]. For interactions between Cu and O, ϵ and σ were set as

$$\sigma_{Cu-O} = \frac{1}{2}(\sigma_{Cu-Cu} + \sigma_{O-O}) \quad (2)$$

$$\epsilon_{Cu-O} = c\sqrt{\epsilon_{Cu-Cu}\epsilon_{O-O}} \quad (3)$$

The wettability of surfaces was established by changing the potential parameter c , representing the effect strength between the solid and liquid [34]. It is known that the contact angle decreases with c [35]. c was set to 1 in all simulations, and the solid and liquid showed a real interaction effect with a contact angle of about 87° , which was larger than the experimental value (76°) [36]. This is due to the roughness of the smooth copper surface in the experiment, which made the experimental surface more hydrophilic [37].

Another potential function is L–J with long-range Coulombic interactions, which was successfully used to describe the interaction forces between H–O, H–H, and O–O atoms [38]:

$$U_{ab} = \sum_i \sum_j \frac{k_c q_{a_i} q_{b_j}}{r_{a_i b_j}} + \sum_i \sum_j 4\epsilon_{a_i b_j} \left[\left(\frac{\sigma_{a_i b_j}}{r_{a_i b_j}} \right)^{12} - \left(\frac{\sigma_{a_i b_j}}{r_{a_i b_j}} \right)^6 \right] \quad (4)$$

The subscripts a and b represent different atom types. The subscripts i and j denote H or O atoms in an individual TIP4P water molecule. q_i is the electric charge of site i , and $r_{a_i b_j}$ denotes the distance between two atoms, a and b . k_c represents the electrostatic constant. The electrostatic potential allows the long-range effect to be presented by the particle–particle particle–mesh model with an accuracy of 10^{-6} . The pair potential between oxygen atoms was set as a cutoff radius of 12 Å.

An artificial harmonic bond between copper atoms was established to prevent the Cu atoms from migrating. An applicable spring constant k closely related to Young's modulus E was established to obtain a temperature that was accurate enough. This can be represented by the following equation [38]:

$$k = Ed \quad (5)$$

where d denotes the lattice constant and E is the Young's modulus for copper. The SHAKE [39] algorithm was applied to maintain the rigidity of the water molecules. The copper–oxygen and water potential parameters are shown in Table 1.

Table 1. Copper–oxygen and water potential parameters.

Parameter	Value	Units
ϵ_{O-O}	0.006998	eV
σ_{O-O}	3.16438	Å
q_O	−1.04	e
q_H	0.52	e
ϵ_{Cu-O}	0.06387	eV
σ_{Cu-O}	2.7172	Å
E	274–306	GPa
d	3.615	Å

3. Results and Discussion

3.1. Snapshot Analysis of Water Molecular Movement

The snapshots taken for four cases during boiling are given in Figure 2 to show the dynamic behaviors of water molecules. At 0 ps, the copper nanochannels were flooded by 5916 water molecules in case 2 (Figure 2b) but were not fully submerged by 4760 water molecules in case 1 (Figure 2a). Meanwhile, the water molecules near the nanochannels appeared denser due to the hydrophilic effect of nanochannels. Water molecules next to the copper nanochannels formed a microfluidic layer, which grew thicker in cases 3 and 4 as the number of water molecules increased from 7072 (Figure 2c) to 8228 (Figure 2d).

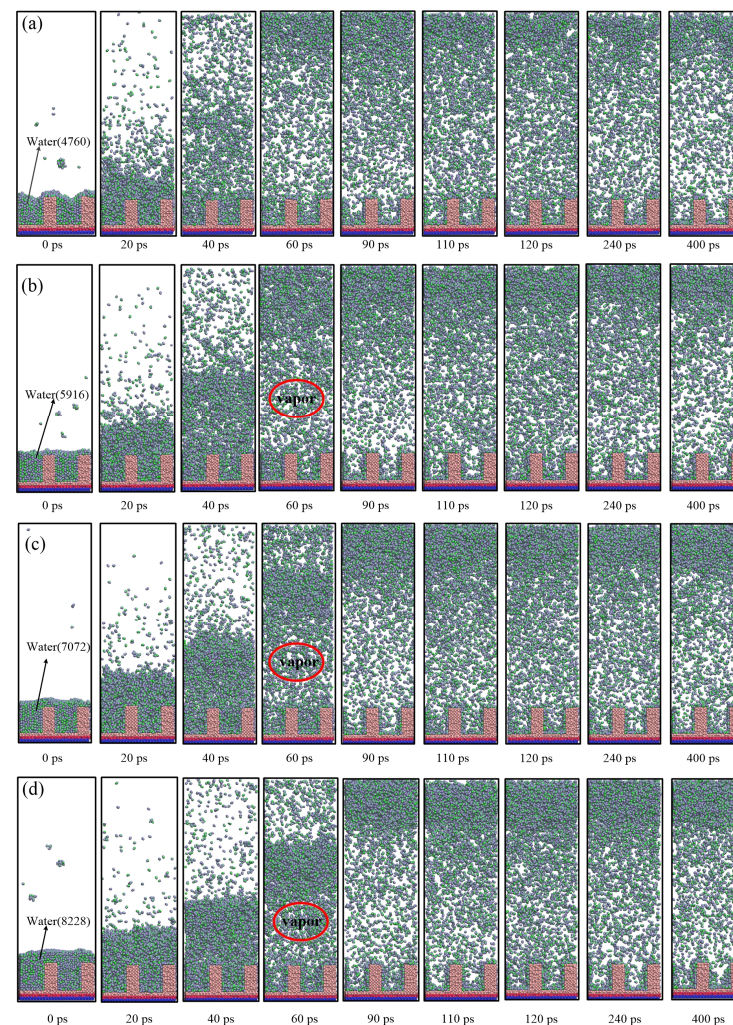


Figure 2. Snapshots with differing numbers of water molecules during rapid boiling: cases (a) 1, (b) 2, (c) 3, and (d) 4.

After 40 ps, the water film detached from the nanochannel copper plate as a liquid cluster and gradually evaporates into the top of the simulation box in cases 2–4. In case 1, the water film directly evaporated into a vaporous phase in the simulation box. When the liquid cluster hit the top of the box, the entire water domain separated into three zones: liquid clusters from the bottom of the box to the top wall, microfluid next to the solid surface, and vapor as marked by the red ellipses. It was noted that the liquid cluster was more pronounced, the liquid water molecules were denser near the nanochannels, and the velocity of the liquid molecules was significantly lower in case 4, which had the most water molecules.

3.2. Density Variations in Water Molecules during Boiling

The computational domain along the Z-direction was divided into 68 bins (length interval 4 Å), and the number of molecules in each bin was calculated to obtain the average water density to study variations in the Z-direction between the four cases. Figure 3 illustrates the effect of different liquid water thicknesses on the density profile for different time periods after the onset of boiling. As shown in Figure 3a, the water evaporated rapidly after 20 ps, and the density was less than 0.1 g/cm³ above a height of 50 Å. From 40 ps to 90 ps, a liquid water peak (marked by the red circle), as shown in Figure 3b–d, which corresponds to the liquid cluster in Section 3.1, gradually moved along the Z-axis until it reached the top of the box. The liquid water peaks from cases 2 to 4 were approximately 0.2, 0.35, and 0.5 g/cm³, respectively. This liquid water peak did not form in case 1 because there was too low a quantity of liquid water, and it quickly evaporated into water vapor.

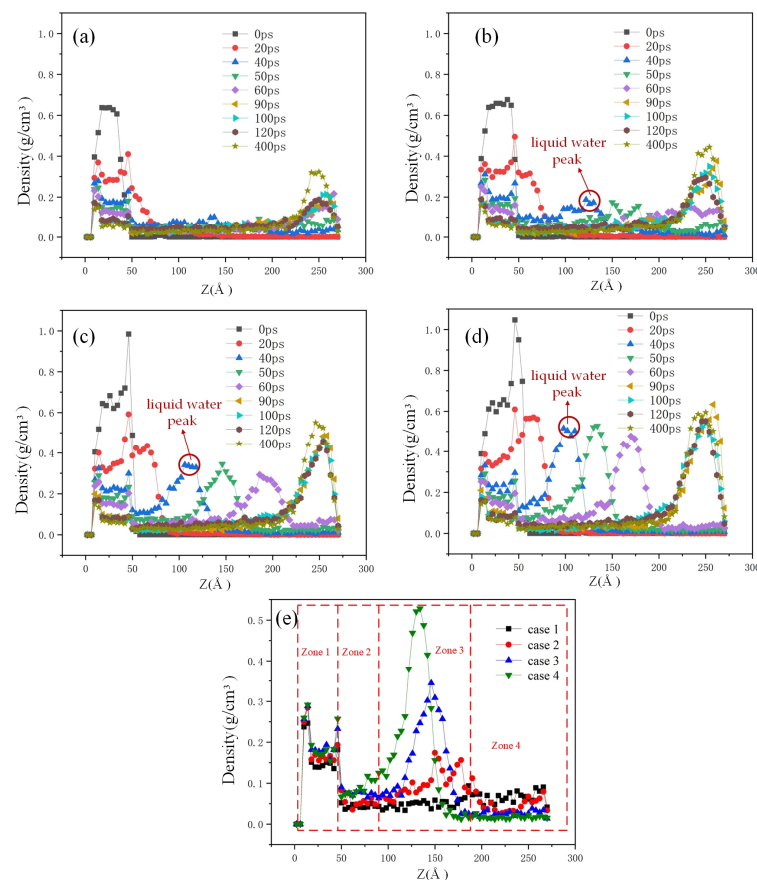


Figure 3. Density variations in water in the Z-direction with different liquid water thicknesses in the rapid boiling process: (a) case 1, (b) case 2, (c) case 3, and (d) case 4, and (e) water molecular density distribution in all cases at 50 ps.

Density profiles for the four cases at 50 ps are shown in Figure 3e. The density division contains four different zones, including the microfluidic zone in the nanochannels (zone 1), the vapor–liquid interface zone on the nanochannels (zone 2), the liquid–phase zone with a relatively high density (except case 1) in the nanochannels (zone 3), and the vapor zone on the top of the box (zone 4), shown as the red dotted box. What is more, from case 1 to case 4, the density of water molecules gradually increased as the number of water molecules increased in zones 1–3. As shown in Figure 3a–d, the density of water in zone 1 (Z coordinates approximately 0–50 Å) decreased over time in every case due to the evaporation of liquid water near the nanochannels. The z-coordinate represents the location of moving liquid water at different times, while the x-coordinate represents the density. The peak of the curve is the density of the liquid water cluster, while the corresponding abscissa is its position. The liquid water cluster peak was the highest in case 4, with a value of around 0.55 g/cm^3 . The departure velocity of the water molecular cluster decreased with the number of water molecules.

3.3. Variations in Copper and Water Temperatures during Boiling

Temperature variations in the copper and water during rapid boiling in all cases are shown in Figure 4. The copper temperature under all conditions rapidly decreased to about 810 K in a short period because of the heat transfer from copper to water, while the corresponding temperature of water rapidly rose to 700–800 K. The copper temperature gradually increased within 150 ps due to the temperature on the two middle layers of the copper atoms, while the water temperature under all working conditions was at the maximum. The water temperature then began to drop due to evaporation. In Figure 4a, the change in copper temperature from case 2 to case 4 is not obvious. However, the copper temperature in case 1 decreased to its lowest value under the same heat source conditions. In Figure 4b, the water temperature can be seen to decrease with the number of water molecules during the entire heat transfer process, which is consistent with the law of energy conservation.

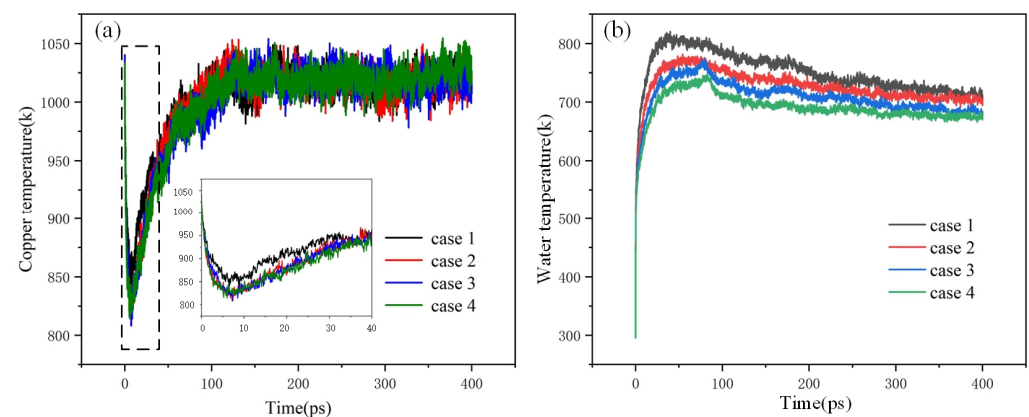


Figure 4. Temperature variations in (a) copper and (b) water for all cases.

The liquid in case 1 vaporized within 50 ps, as shown in Figure 2a of Section 3.1, and the density of water in case 1, which was in contact with hot copper, also had the lowest value, as shown in Figure 3e of Section 3.2. There was not enough liquid water to touch the copper for evaporation in case 1. Therefore, when insufficient liquid water molecules covered the nanochannels, the surface heat transfer effect worsened. It can be inferred from the cooling effect of copper that the heat transfer effect in case 1 was the worst.

3.4. Evaporation Rate Variation during Boiling

The evaporation rate is defined as the ratio of water molecules during the vapor phase to those in the initial liquid water during boiling. The evaporation of water molecules and the evaporation rate under the four working conditions are compared in Figure 5. As shown

in Figure 5a, the number of water molecules increased rapidly in all cases within 50 ps, and the water clusters rose to the top of the simulated box before bouncing back. The water vapor flow was obstructed, causing liquid blockage due to rapid water evaporation [40] at around 50 ps. Thus, evaporation fluctuated after falling and then rose to between 50 and 150 ps before steadily decreasing after 200 ps.

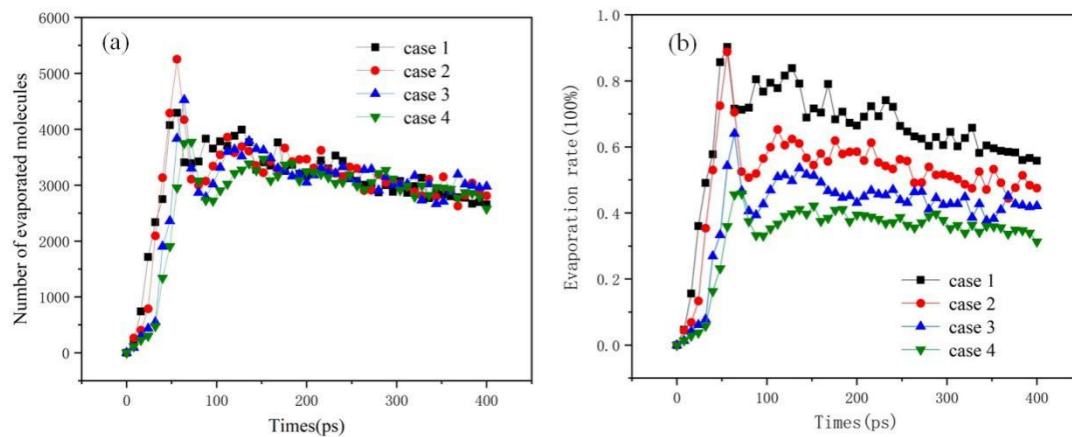


Figure 5. (a) Variations in the number of evaporated molecules and (b) the evaporation rate of water for all cases.

In case 2, the number of evaporated molecules had a maximum value (5252) around 50 ps and was larger than all other cases. As shown in Figure 5b, it is important that the maximum evaporation rates of cases 1 and case 2 were similar (about 90%) at 50 ps, but the number of water molecules evaporated in case 2 was about 1000 more than that in case 1. The reason why the evaporation amount in case 2 was larger than in that in case 1 can be inferred to be due to the fact that there were not enough water molecules in case 1 to come into contact with the hot copper. The water evaporation rate in case 3 was about 65% and peaked at 70 ps, while the evaporation rate of case 4 was about 45% at 70 ps. Between 50 ps and 90 ps, the maximum evaporation rate of water in case 2 was 25% and 45% higher than that in cases 3 and 4, respectively. After 100 ps, the evaporation rate of water was directly related to the initial number of water molecules, and the evaporation rate of water molecules was lower with a higher number of water molecules. In conclusion, the number of evaporated molecules in case 2, where water molecules just covered the nanochannels of copper, was higher than that in other cases.

3.5. Analysis of Microfluid Flow in Vapor–Liquid Coexisting near the Nanochannel Surface

As described in Section 3.4, there is a critical relationship between the heat transfer characteristics of water films with different thicknesses and the microfluid flow near nanochannel surfaces. The potential energy, kinetic energy, and density distribution of water molecules near nanochannels were analyzed at 50 ps, as shown in Figure 6, to study the vapor–liquid flow mechanism on the nanochannel surface (the zone shown in the red dotted box in Figure 6a) during rapid boiling.

Figure 6b shows that the water density in case 1 was the lowest, followed by case 2. The water densities were similar in cases 3 and 4. As can be seen in Figure 6c,d, the kinetic and potential energies of water in all cases showed the same trend in the concave and convex regions of the nanochannels. The kinetic energy and the absolute value of the potential energy in the concave (convex) regions of the nanochannels were low (high). The potential energy differences increased when there were fewer water molecules in the same plane region in the concave and convex regions of the nanochannels. An interesting phenomenon is that the kinetic and potential energy of water molecules was obviously different in different cases between the convex and concave region of the nanochannels. The energy difference existed in the vapor–liquid coexistence zone on the nanochannels, and the energy difference increased with the decrease in the liquid film thickness. The

high kinetic energy in the convex area was due to the heat transfer from copper to water in contact with the hot copper. The absolute value of the potential energy was low (weak attraction) in the concave region because nucleation points were formed there.

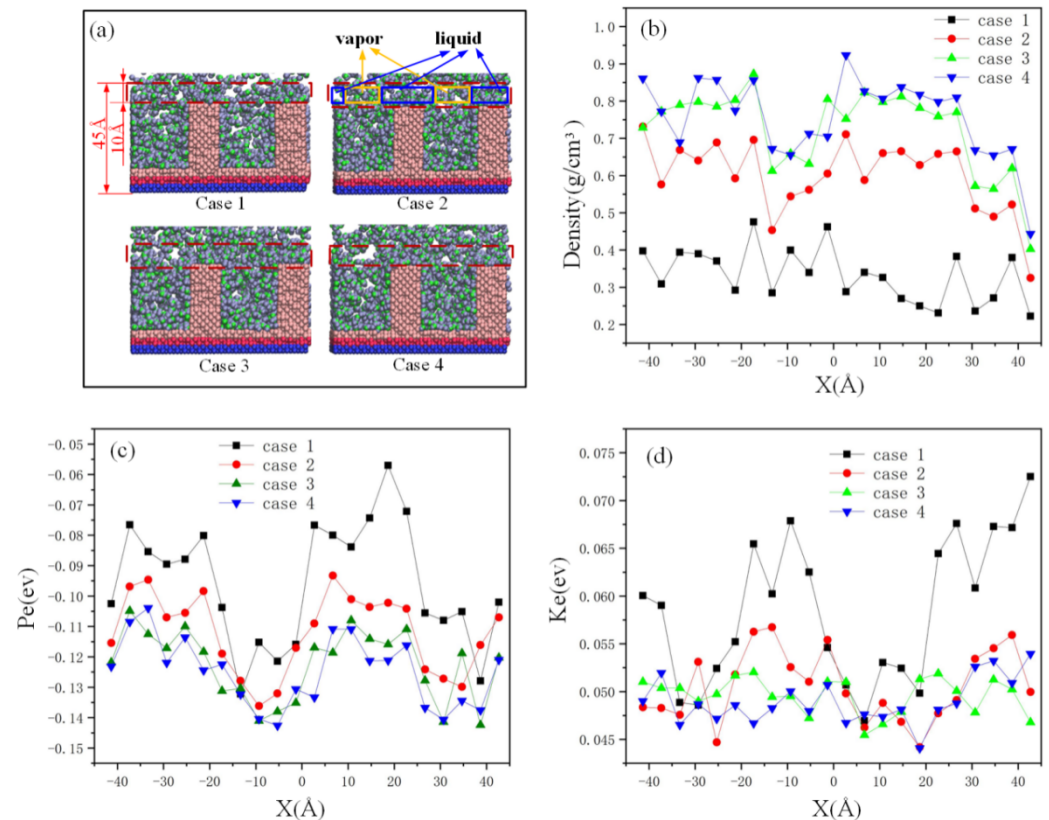


Figure 6. Comparison of water molecule parameters near nanochannels at 50 ps for all cases: (a) distribution, (b) density plot, (c) potential energy (Pe), and (d) kinetic energy (Ke).

The low density of water molecules in the concave area was determined to be the vapor phase area, which is considered the nucleation point [41], as shown in Figure 7a–d with yellow ellipses. As can be seen in Figure 7e, which describes the density of water from 5 Å to 42 Å along the Z-direction, the density of water was the lowest in case 1. This is followed by case 2. Moreover, the density values of case 3 and case 4 were the highest and were similar. Therefore, the microfluidic flow layer was the thinnest in case 1, followed by case 2. Case 3 and case 4 had the thickest layer and were similar. With differing numbers of water molecules, microfluidic flows of different thicknesses formed above the nanochannels, as shown in the red box in Figure 7a–d. The yellow circles of low-density water indicate the nucleation points. The blue arrows illustrate water molecules flowing from microfluid locations to nucleation points. This result is consistent with and successfully explains what Yang et al. [42] proved by experiment: the internal circulation of evaporator can be driven by a phase transition composed of a vapor–liquid interface, and this internal driving force plays an important role in the operation performance of an evaporator. The heat transfer performance of the nanochannel surfaces depends on the potential energy difference between the nucleating point and microfluid flow, where the vapor and liquid coexist, as shown in the blue and yellow dotted boxes in Figure 6a. At the same time, it is necessary to ensure sufficient working liquid flows to the nucleation point for liquid replenishment. Thus, the maximum evaporation in case 2 was caused by the combination of a larger potential energy difference and a microfluid flow with a certain thickness.

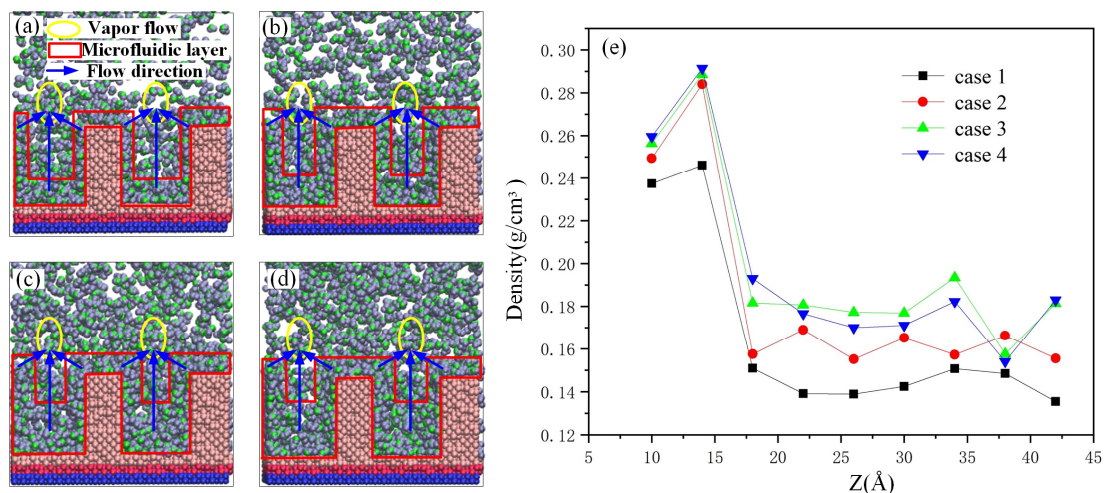


Figure 7. Analysis of microfluid flow in the liquid film for different thicknesses near nanochannels: cases (a) 1, (b) 2, (c) 3, and (d) 4, and (e) the density of water along the Z-direction near the nanochannels.

4. Conclusions

In this study, the effect of different water film thicknesses on rapid boiling was studied through MD simulations. Heat transfer phenomena via phase changes in water films with four different thicknesses were evaluated and compared, including solid–liquid temperature changes, evaporation rate variations, and microfluidic dynamic analyses near surfaces. The main conclusions are given as follows:

- (1) The copper temperature dropped in all cases, while the water temperature rose rapidly within 10 ps. The water temperature increased as the water film thickness decreased. In case 1, the copper temperature was the greatest, and the heat transfer was the worst when the water film thickness was thinner than in the other cases. This is because there was too little working fluid for replenishment to the nucleation point.
- (2) A large water cluster, which formed in each case except case 1, separated from the copper plate heat source through vapor molecules, and the water cluster volume increased with the water film thickness if the nanochannels' copper plate was completely covered by water (cases 2–4). The liquid plug phenomenon in the narrow space affected the continuous supply of liquid water and evaporation of the nucleation points in the nanochannels.
- (3) The large potential energy difference in the vapor–liquid coexistence zone on the nanochannels promoted the vapor–liquid flow, which has a great influence on the enhancement of heat transfer. Heat transfer performance was the best in case 2 when there was enough liquid water and a large potential energy difference. The maximum evaporation rate of water in case 2 was 25%, 45% higher than that in cases 3 and 4, respectively. The number of water molecules evaporated in case 2 was the highest and about 1000 more than that in case 1.

Author Contributions: N.W.: writing—review and editing, methodology and visualization. L.Z.: methodology and investigation. T.F.: methodology and supervision. J.C.: conceptualization and supervision. F.Z.: validation and formal analysis. Y.Z.: methodology and writing—review and editing. S.P.: writing—original draft and formal analysis. All authors have read and agreed to the published version of the manuscript.

Funding: This research was financially supported by the National Natural Science Foundation of China (grant no. 51975425 and no. 12102311) and the Open Fund of Hubei Key Laboratory of Mechanical Transmission and Manufacturing Engineering at Wuhan University of Science and Technology (MTMEOF2022B01).

Institutional Review Board Statement: Not applicable.

Informed Consent Statement: Not applicable.

Data Availability Statement: The data that support the results of this study can be made available by the corresponding author upon reasonable request.

Conflicts of Interest: The authors declare no conflict of interest.

References

- Carey, V.P. *Liquid Vapor Phase Change Phenomena: An Introduction to the Thermophysics of Vaporization and Condensation Processes in Heat Transfer Equipment*; Taylor&Francis Group: New York, NY, USA, 2008.
- Goldstein, R.J.; Ibele, W.E.; Patankar, S.V.; Simon, T.W.; Kuehn, T.H.; Strykowski, P.J.; Tamma, K.K.; Heberlein, J.V.R.; Davidson, J.H.; Bischof, J.; et al. Heat transfer—A review of 2004 literature. *Int. J. Heat Mass Transf.* **2010**, *53*, 4343–4396. [\[CrossRef\]](#)
- Tang, H.; Tang, Y.; Wan, Z.; Li, J.; Yuan, W.; Lu, L.; Li, Y.; Tang, K. Review of applications and developments of ultra-thin micro heat pipes for electronic cooling. *Appl. Energy* **2018**, *223*, 383. [\[CrossRef\]](#)
- Deng, D.; Zeng, L.; Sun, W. A review on flow boiling enhancement and fabrication of enhanced microchannels of microchannel heat sinks. *Int. J. Heat Mass Transf.* **2021**, *175*, 121332. [\[CrossRef\]](#)
- Chen, G.; Tang, Y.; Duan, L.; Tang, H.; Zhong, G.; Wan, Z.; Zhang, S.; Fu, T. Thermal performance enhancement of micro-grooved aluminum flat plate heat pipes applied in solar collectors. *Renew. Energy* **2020**, *146*, 2234–2242. [\[CrossRef\]](#)
- Kim, M.-W.; Kim, T.G.; Jo, H.S.; Lee, J.-G.; James, S.C.; Choi, M.S.; Kim, W.Y.; Yang, J.S.; Choi, J.; Yoon, S.S. Nano-textured surfaces using hybrid micro- and nano-materials for efficient water cooling. *Int. J. Heat Mass Transf.* **2018**, *123*, 1120–1127. [\[CrossRef\]](#)
- Zhang, L.; Wang, T.; Jiang, Y.; Kim, S.; Guo, C. A study of boiling on surfaces with temperature-dependent wettability by lattice Boltzmann method. *Int. J. Heat Mass Transf.* **2018**, *122*, 775–784. [\[CrossRef\]](#)
- Kim, D.E.; Yu, D.I.; Jerng, D.W.; Kim, M.H.; Ahn, H.S. Review of boiling heat transfer enhancement on micro/nanostructured surfaces. *Exp. Therm. Fluid Sci.* **2015**, *66*, 173–196. [\[CrossRef\]](#)
- Cao, Z.; Wu, Z.; Pham, A.-D.; Yang, Y.; Abboud, S.; Falkman, P.; Ruzgas, T.; Albèr, C.; Sundén, B. Pool boiling of HFE-7200 on nanoparticle-coating surfaces: Experiments and heat transfer analysis. *Int. J. Heat Mass Transf.* **2019**, *133*, 548. [\[CrossRef\]](#)
- Liu, B.; Liu, J.; Zhou, J.; Yuan, B.; Zhang, Y.; Wei, J.; Wang, W. Experimental study of subcooled boiling pool heat transfer and its “hook back” phenomenon on micro/nanostructured surfaces. *Int. Commun. Heat Mass Transf.* **2019**, *100*, 73–82. [\[CrossRef\]](#)
- Shen, C.; Zhang, C.; Bao, Y.; Wang, X.; Liu, Y.; Ren, L. Experimental investigation on enhancement of nucleate pool boiling heat transfer using hybrid wetting pillar surface at low heat fluxes. *Int. J. Therm. Sci.* **2018**, *130*, 47–58. [\[CrossRef\]](#)
- Chen, L.; Wang, S.-Y.; Xiang, X.; Tao, W.-Q. Mechanism of surface nanostructure changing wettability: A molecular dynamics simulation. *Comput. Mater. Sci.* **2020**, *171*, 109223. [\[CrossRef\]](#)
- Zhao, Z.; Zhang, J.; Jia, D.; Zhao, K.; Zhang, X.; Jiang, P. Thermal performance analysis of pool boiling on an enhanced surface modified by the combination of microstructures and wetting properties. *Appl. Therm. Eng.* **2017**, *117*, 417–426. [\[CrossRef\]](#)
- Phan, H.T.; Caney, N.; Marty, P. Surface wettability control by nanocoating: The effects on pool boiling heat transfer and nucleation mechanism. *Int. J. Heat Mass Transf.* **2009**, *52*, 5459–5471. [\[CrossRef\]](#)
- Milczarek, M.; Jarzabek, D.M.; Jenczyk, P.; Bochenek, K.; Filipiak, M. Novel paradigm in AFM probe fabrication: Broadened range of stiffness, materials, and tip shapes. *Tribol. Int.* **2023**, *180*, 108308. [\[CrossRef\]](#)
- Yin, X.; Hu, C.; Bai, M.; Lv, J. Molecular dynamic simulation of rapid boiling of nanofluids on different wetting surfaces with depositional nanoparticles. *Int. J. Multiph. Flow* **2019**, *115*, 9–18. [\[CrossRef\]](#)
- Liu, H.; Ahmad, S.; Chen, J.; Zhao, J. Molecular dynamics study of the nanoscale boiling heat transfer process on nanostructured surfaces. *Int. Commun. Heat Mass Transf.* **2020**, *119*, 104963. [\[CrossRef\]](#)
- Hens, A.; Agarwal, R.; Biswas, G. Nanoscale study of boiling and evaporation in a liquid Ar film on a Pt heater using molecular dynamics simulation. *Int. J. Heat Mass Transf.* **2014**, *71*, 303–312. [\[CrossRef\]](#)
- Wang, W.; Huang, S.; Luo, X. MD simulation on nano-scale heat transfer mechanism of sub-cooled boiling on nano-structured surface. *Int. J. Heat Mass Transf.* **2016**, *100*, 276–286. [\[CrossRef\]](#)
- Zhang, S.; Hao, F.; Chen, H.; Yuan, W.; Tang, Y.; Chen, X. Molecular dynamics simulation on explosive boiling of liquid argon film on copper nanochannels. *Appl. Therm. Eng.* **2017**, *113*, 208–214. [\[CrossRef\]](#)
- Shavik, S.M.; Hasan, M.N.; Monjur Morshed, A.K.M. Molecular Dynamics Study on Explosive Boiling of Thin Liquid Argon Film on Nanostructured Surface under Different Wetting Conditions. *J. Electron. Packag.* **2016**, *138*, 010904. [\[CrossRef\]](#)
- Li, L.; Ji, P.; Zhang, Y. Molecular dynamics simulation of condensation on nanostructured surface in a confined space. *Appl. Phys. A* **2016**, *122*, 496. [\[CrossRef\]](#)
- Li, X.; Cole, I.; Tu, J. A review of nucleate boiling on nanoengineered surfaces—The nanostructures, phenomena and mechanisms. *Int. J. Heat Mass Transf.* **2019**, *141*, 20–33. [\[CrossRef\]](#)
- Eid, M.M.A.A.; Zubir, M.N.M.; Muhamad, M.R.; Kazi, S.N.; Aznam, S.M.; Rony, M.H.; Ibrahim, F.A.; Alam, M.S.; Sadri, R. Experimental and numerical investigations on the effect of a novel internal surface micro-grooving toward improving convective heat transfer performance of tube heat exchangers. *Phys. Fluids* **2023**, *35*, 075114. [\[CrossRef\]](#)
- Chen, Y.; Zou, Y.; Sun, D.; Wang, Y.; Yu, B. Molecular dynamics simulation of bubble nucleation on nanostructure surface. *Int. J. Heat Mass Transf.* **2018**, *118*, 1143–1151. [\[CrossRef\]](#)
- Fan, J.; Wu, H.; Wang, F. Evaporation-driven liquid flow through nanochannels. *Phys. Fluids* **2020**, *32*, 012001. [\[CrossRef\]](#)

27. Hanks, D.F.; Lu, Z.; Sircar, J.; Salamon, T.R.; Antao, D.S.; Bagnall, K.R.; Barabadi, B.; Wang, E.N. Nanoporous membrane device for ultra high heat flux thermal management. *Microsyst. Nanoeng.* **2018**, *4*, 1. [[CrossRef](#)] [[PubMed](#)]
28. Li, J.; Chen, J.; Chen, Y.; Luo, X.; Liang, Y.; Yang, Z. Effectiveness of actively adjusting vapour liquid in the evaporator for heat transfer enhancement. *Appl. Therm. Eng. Des. Process. Equip. Econ.* **2022**, *200*, 117696. [[CrossRef](#)]
29. Jorgensen, W.L.; Madura, J.D. Temperature and size dependence for Monte Carlo simulations of TIP4P water. *Mol. Phys.* **1985**, *56*, 1381–1392. [[CrossRef](#)]
30. Mahoney, M.W.; Jorgensen, W.L. A five-site model for liquid water and the reproduction of the density anomaly by rigid, nonpolarizable potential functions. *J. Chem. Phys.* **2000**, *112*, 8910. [[CrossRef](#)]
31. Humphrey, W.; Dalke, A.; Schulten, K. VMD: Visual molecular dynamics. *J. Mol. Graph.* **1996**, *14*, 33–38. [[CrossRef](#)]
32. Zarringhalam, M.; Ahmadi-Danesh-Ashtiani, H.; Toghraie, D.; Fazaali, R. Molecular dynamic simulation to study the effects of roughness elements with cone geometry on the boiling flow inside a microchannel. *Int. J. Heat Mass Transf.* **2019**, *141*, 1–8. [[CrossRef](#)]
33. Zhang, P.; Jin, L.; Zhou, L.; Du, X.; Yang, Y. Heat transfer around copper nanoparticle with high superheat in water pool: A molecular dynamics simulation. *Therm. Sci. Eng. Prog.* **2018**, *8*, 509–516. [[CrossRef](#)]
34. Isaiev, M.; Burian, S.; Bulavin, L.; Gradeck, M.; Lemoine, F.; Termentzidis, K. Efficient tuning of potential parameters for liquid–solid interactions. *Mol. Simul.* **2015**, *42*, 910–915. [[CrossRef](#)]
35. Diaz, R.; Guo, Z. Molecular dynamics study of wettability and pitch effects on maximum critical heat flux in evaporation and pool boiling heat transfer. *Numer. Heat Transf. Part A Appl.* **2017**, *72*, 891–903. [[CrossRef](#)]
36. Wu, N.; Zeng, L.; Chen, J.; Fu, T.; Zhang, F.; Zeng, Y. Influence of Tuning Potential Parameters on Wettability of Smooth Copper Plate: A Molecular Dynamic Study. *Coatings* **2023**, *13*, 1371. [[CrossRef](#)]
37. Fu, T.; Wu, N.; Lu, C.; Wang, J.; Wang, Q. Effect of nanostructure on wettability on copper surface: A molecular dynamic study. *Mol. Simul.* **2018**, *45*, 35–39. [[CrossRef](#)]
38. Mao, Y.; Zhang, Y. Molecular dynamics simulation on rapid boiling of water on a hot copper plate. *Appl. Therm. Eng.* **2014**, *62*, 607–612. [[CrossRef](#)]
39. Ryckaert, J.P.; Ciccotti, G.; Berendsen, H.J. Numerical Integration of the Cartesian Equations of Motion of a System with Constraints: Molecular Dynamics of n-Alkanes. *J. Comput. Phys.* **1977**, *23*, 327–341. [[CrossRef](#)]
40. Li, W.; Wang, Z.; Yang, F. Supercapillary architecture-activated two-phase boundary layer structures for highly stable and efficient flow boiling heat transfer. *Adv. Mater.* **2020**, *32*, 1905117. [[CrossRef](#)]
41. Wu, N.; Zeng, L.; Fu, T.; Wang, Z.; Lu, C. Molecular dynamics study of rapid boiling of thin liquid water film on smooth copper surface under different wettability conditions. *Int. J. Heat Mass Transf.* **2020**, *147*, 118905. [[CrossRef](#)]
42. Yang, Y.; Zhu, K.; Wang, Y.; Wei, J.; Zheng, M.; Cui, Z. Experimental investigation and visual observation of a vapor–liquid separated flat loop heat pipe evaporator. *Appl. Therm. Eng.* **2016**, *101*, 71–78. [[CrossRef](#)]

Disclaimer/Publisher’s Note: The statements, opinions and data contained in all publications are solely those of the individual author(s) and contributor(s) and not of MDPI and/or the editor(s). MDPI and/or the editor(s) disclaim responsibility for any injury to people or property resulting from any ideas, methods, instructions or products referred to in the content.